SAND--90-1923C

DE90 014998

CONF-9009192--5

CHARACTERIZATION OF ELECTRON FLOW IN POSITIVE-POLARITY LINEAR-INDUCTION ACCELERATORS

S. E. Rosenthal
Pulsed Power Theory Division
Sandia National Laboratories
Albuquerque, NM 87185

Abstract

Experiments at Sandia National Laboratories have studied the operation of the linear-induction accelerators, HELIA[1] and Hermes III[2], in positive polarity. These experiments have provided a unique opportunity to explore the consequences of multiple-cathode electron emission in magnetically insulated transmission lines. An examination of the total energy-canonical momentum distribution of the electrons explains the features of the magnetically insulated flow exhibited by these systems. Simple analysis based on the basic concept of pressure balance, in conjunction with particle-in-cell numerical simulations, shows how the line voltage is related to the anode and cathode currents. Two flow designations are introduced that can apply to multiple-cathode magnetically insulated transmission lines: full-gap flow (FGF), and locally emitted flow (LEF).

Introduction

Hermes III was designed to operate in negative polarity to power electron beam diodes for gamma ray production[3]. Its pulse is 40 ns wide with a peak-voltage operating point at 730 kA, 22 MV. This voltage is produced by the series voltage addition that occurs along the power flow direction in a coaxial magnetically insulated transmission line (MITL). Properly timed pulses arrive at the MITL via radial disk power feeds. This type of accelerator can also be used in positive polarity to power ion diodes used in ICF research[3-6].

The essential difference between negative and positive polarities in this accelerator is that the cathode is one continuous conductor, the inner line of the coaxial MITL, in negative polarity; while, in positive polarity the cathode includes the sections of the outer line of the MITL that are between the radial disk feeds, and is thus split into 20 separate conductors.

A concern with how the MITL voltage on positive-polarity Hermes III or HELIA (a prototype having 4 radial disk power feeds) might be determined from the anode and cathode dB/dt signals has led to an investigation of the basic features of the electron flow that occur in the MITLs of multiple-cathode accelerators. In the positive-polarity Hermes III, for example, there are 20 distinct classes of electrons comprising the flow in the final MITL, one from each cathode. Because of this feature the simple magnetically insulated flow models for cylindrical MITLs[7-10] cannot be applied in the usual way. The particle-in-cell code, MAGIC[11] has been used to numerically simulate the Hermes-III system in positive polarity. These MAGIC simulations show that if the anode and cathode currents are used to calculate the line voltage in the usual way, the calculated voltage is substantially greater (about 75%) than the correct value.

As shown in this paper, taking care in the voltage calculation to address the presence of the electron flow that is injected into the final MITL from all the upstream sections of the voltage adder gives the correct voltage for the MAGIC simulations. Presumably, the correct voltage for the experiments can be obtained in the same way. Two different methods have been studied and will be described.

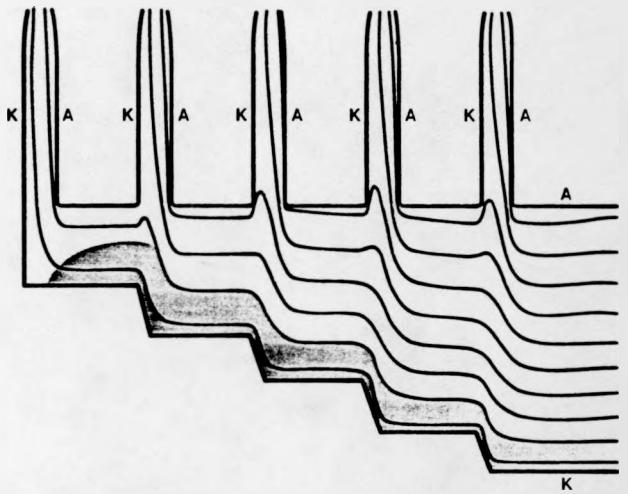

Fig. 1. Idealized negative-polarity voltage adder geometry illustrating band of parapotential flow near the single, continuous cathode.

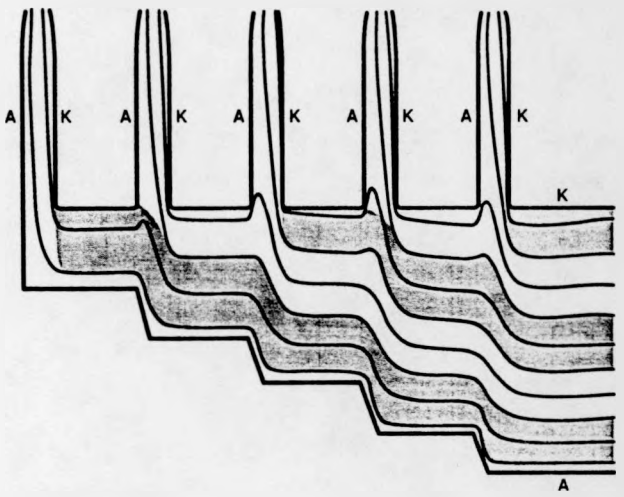

Fig. 2. Idealized positive-polarity voltage adder geometry illustrating bands of parapotential flow from multiple cathodes.

The idealized voltage adder geometry (used in the simulations) of Fig. 1 or Fig. 2 shows the vacuum equipotential surfaces at a time when all the pulses have arrived at the final MITL at full amplitude. This illustrates how the voltage addition occurs. Note that the voltage across the final MITL gap is the sum of the voltages of each of the feed gaps. The final MITL continues to the right, but is not shown in these figures; nor is the full radial height of the disk feeds. Each of the radial disk feeds represents 4 Hermes-III feeds. In negative polarity the cathode is a single, continuous

---

conductor, and it is related to the same set of equipotentials all the way along the adder to the final MITL. The shaded area of Fig. 1 qualitatively shows the pattern for electron flow that is characterized by E x B drift along equipotential surfaces when the polarity is negative. Such a flow remains continuous throughout the adder to the final MITL.

Now, in positive polarity the cathode is split into separate sections, each related to a different set of equipotentials. The alternate light and dark shaded areas of Fig. 2 illustrate the likely parapotential flow regions from each cathode. By the final MITL the flow will extend across the entire gap based on this simple view. The self-consistent interaction between the fields and electrons does not change this conclusion substantially.

1-D Equilibrium MITL Theory

One-dimensional, equilibrium magnetic insulation theory has proven to be useful and quite successful in the negative-polarity Hermes-III design and data analysis. As an important first step in understanding how Hermes III works in positive polarity, we need to learn to what extent, if any, the simple theory that is successful in negative polarity (single cathode), applies. A theory is needed to enable us to characterize the electron flows in positive polarity. 2-D, fully electromagnetic particle-in-cell simulations guide us in this effort.

We use the Magnetic Insulation Code, MAGIC. This particle-in-cell (PIC) code is fully electromagnetic (2-D field solver, 6 field components), with 3-D relativistic particle kinematics. In these simulations electrons enter the system through a simple Gauss's law model for space-charge-limited emission from the negative electrodes. The reader should refer to [11] for a more complete description of this code.

Pressure Balance Theory

Let us first review an example of 1-D magnetic insulation theory. This particular example[7-9] makes use of the pressure balance between the anode and cathode during magnetically insulated equilibrium. The model assumes that at equilibrium the electron cloud as a whole travels parallel to the electrodes and is accelerated toward neither. No particular type of orbit is assumed for all the electrons within the cloud. Assuming additionally that (1) the entire cathode defines a single equipotential surface, (2) the normal cathode electric field is zero (space-charge-limited electron emission), (3) the electron charge density is constant across the flow, and (4) electrons with zero total energy and axial canonical momentum can leave the cathode on stable laminar orbits, we get a simple relationship between the anode and cathode currents (I_A, I_C) and the line voltage (V).

$$V = Z_0 (I_A^2 - I_C^2)^{1/2} - mc^2/2e\,(I_A^2/I_C^2 - 1) \quad (1)$$

where Z_0 is the vacuum impedance, m the electron rest mass, c the vacuum speed of light, and e the magnitude of the electron charge, all in MKS units. This relationship is for planar geometry, but, with Hermes-III impedances, there is negligible difference from the results of the more elaborate cylindrical expression. The value of the electron charge density implied by assumption (4) is[8]

$$\rho = \epsilon_0 B_C^2\, e/m\,, \qquad (2)$$

where $B_C = (\mu_0 I_C/2\pi r_C)$ is the cathode magnetic field, ϵ_0 is the vacuum permittivity, μ_0 the vacuum permeability, and r the cathode radius. Another way to describe this density is that the electron plasma and cyclotron frequencies are equal at the cathode. MITL simulations support assumptions (3) and (4); and, the voltage for given anode and cathode currents is not sensitive to the precise density profile except for saturated flow[7].

Contours of voltage calculated by (1) plotted in the anode-catho current plane appear as in Fig. 3; where the 4, 8, 12, 16, and 20 MV contours, appropriate for negative-polarity Hermes III, are plotted. Numerical simulations and measurements from many magnetically insulated devices have shown that the self-limited current tends to be near the minimum current on any voltage contour. The locus of the minimum current for all voltages is given by the broken curve of Fig. 3. Hence for any voltage we know the anode current and the corresponding cathode current. The difference between them is the electron flow current, so this theory also gives the electron flow current for any voltage. Voltages and currents that change quasi-statically (timescale ~ ω_C^{-1} ~ 10^{-10} sec) can be accurately described by an equilibrium theory. The Hermes-III pulse, for example, has a ~ 20 ns rise time.

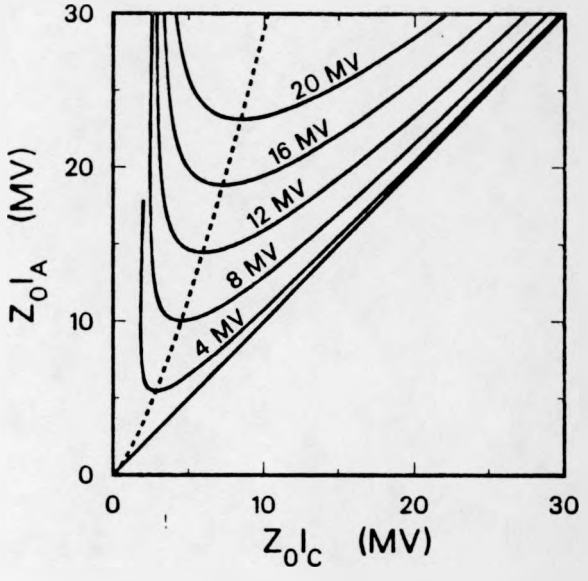

Fig. 3. Voltage contours for 1-D, planar magnetically insulated equilibrium.

Matching Self-Limited Current

In a MITL that has no equilibrium electron loss, the anode current is constant along the length of the MITL. Efficient equilibrium operation of Hermes III requires that the anode current be the same throughout the adder and final MITL. Hermes III has a final MITL that is sufficiently long to isolate the voltage-adder MITL from the terminating diode during the pulse length of the accelerator, so the anode current is determined by the self-limited current of the final MITL. This current is defined by the minimum current of the equilibrium voltage contour for the final-MITL voltage and vacuum impedance. The vacuum impedance Z_0 of each of the preceeding sections of the adder MITL can then be chosen so that the minimum current for each of the section voltages is the same. This choice allows matched self-limited flow for the local voltage and vacuum impedance all the way through the adder to the final MITL. Such an

approach contrasts with the HELIA accelerator which normally has a short final MITL; its current is determined by the terminating diode impedance.

The concept of matching self-limited current was applied to the calculation of the inner radii of each section of negative-polarity Hermes III. The solution for a subset of inner radii is shown in Fig. 4 for an anode current of 750 kA and final MITL voltage of 20 MV. Voltage contours for five sections (these particular sections are called "spools" on Hermes III) are shown: 4, 8, 12, 16, and 20 MV. At any of these sections the inner radius is chosen to give a vacuum impedance such that the anode (outer) current is 750 kA and matches the minimum-current equilibria (triangles of Fig. 4) for the local voltage.

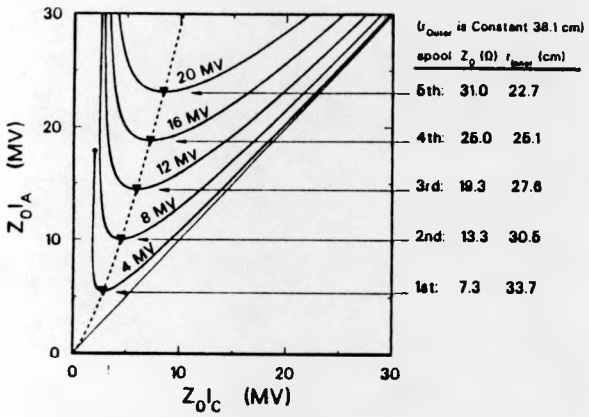

Fig. 4. At any section of negative-polarity Hermes III the anode current is 750 kA and matches the minimum-current equilibria (triangles) for the local voltage and vacuum impedance.

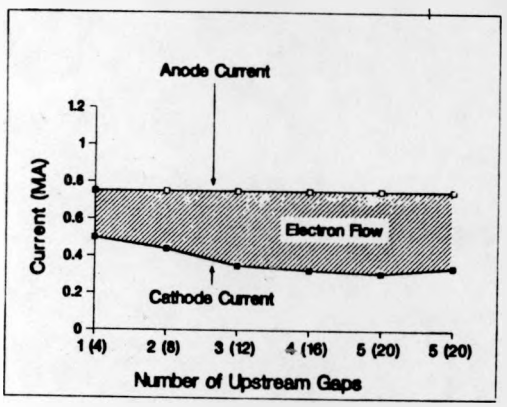

Fig. 5. Electron flow increases slightly with voltage in simulations of negative-polarity Hermes III. The numbers on the abscissa are spool numbers or number of upstream gaps in the simulation; the numbers in parenthases are the corresponding number of Hermes-III gaps. The second 5(20) position is downstream of the first 5(20) position.

The solution is not sensitive to the particular equilibrium flow model used in the voltage contour calculation. For example, the relativistic Brillouin flow and the relativistic quasilaminar flow models[12] give minimum currents that are indistinguishable from the pressure balance results. Matching self-limited currents section to section produces the remarkable result that each section of the MITL behaves like an infinitely long MITL with the local voltage and Z_0.

Negative-polarity Hermes III was designed based on 1-D theory. Simulations[13] and measurements[3] on the completed accelerator have demonstrated the correctness of the matched self-limit current concept.

The Electron Flow Graph of Fig. 5 shows he cathode currents and the constant anode current, 750 kA, from a simulation of negative-polarity Hermes III. The voltage is 20 MV. With the appropriate transit-time corrections, the plotted points occur at the same time in the pulse: when the flow is self limited, and when the voltage is maximum, at each diagnostic location (spool) of the accelerator. The locations match the diagnostic locations of Hermes III. For example, no. 3 is at the center of the spool following the 3rd simulation feed, or equivalently, the 12th Hermes-III feed. Note that the undermatched terminating diode influences the cathode current at position 6 by this time in the simulation. The difference between the two curves is the electron flow current. This increases slightly with voltage or position along the adder in accordance with 1-D theory. Measurements exhibit the same behavior.

Simulations of Positive-Polarity Hermes III

Numerical simulations of Hermes III show the different features of positive polarity. Only 120 cm of the 600-cm length final MITL of Hermes III was included in the simulation. This shorter length provided sufficient isolation from the electron diode termination for 35 ns of self-limited flow at the upstream end of the final MITL. After about 35 ns into the pulse the MITL is load dominated (the terminating electron diode draws more than the self-limited current of the final MITL). Comparison with the experiment is possible during the self-limited portion of the pulse. The simulation calculations include the self-consistent coupling between the electrons and the fields; yet, the results are not qualitatively different from what can be concluded from the vacuum equipotentials.

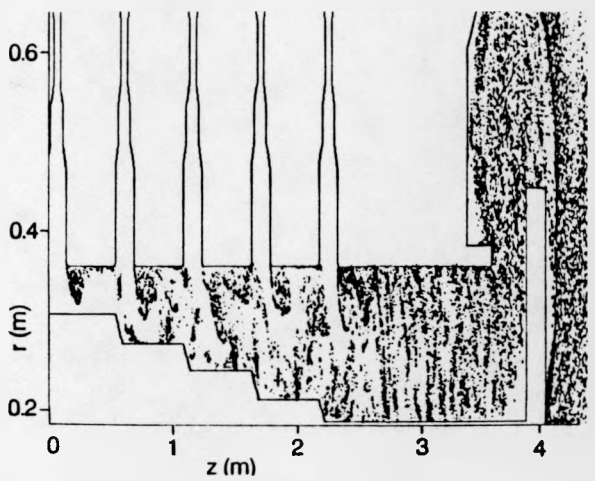

Fig. 6. Positive-polarity simulation particle plot in z-r plane at 22 ns.

Comparison with Negative Polarity

Compared to negative-polarity operation, (a) the electron flow increases more dramatically with voltage, and with the number of cathodes, (b) the final MITL impedance is substantially less for the same voltage, (c) there is turbulence in the adder, and (d) the flow extends across the entire gap of the final MITL. This is the "full-gap" flow (FGF). The locally emitted flow (LEF) of the final MITL comprises about half of the full-gap flow. The locally emitted

electrons would lose the full accelerator energy if lost to the anode, while the other half of the full-gap flow injected into the final MITL from the adder includes many electrons that are close to the anode potential.

z-r Particle Plots

The particle plot of Fig. 6 is from a positive-polarity Hermes III simulation near the time of peak voltage shows some of the features of the electron flow when the final MITL is self limited. A portion of the electron diode load used is included at the right of the picture. Note the turbulence in the adder section. Also, as the vacuum equipotentials suggested, the flow does indeed fill the whole gap of the final MITL.

P_z-W Particle Plots

Another interesting way to view the simulation electrons is in the phase plane of axial canonical momentum and total (kinetic + potential) energy: P_z, W. As discussed in detail in [14], an electron in the flow can occupy only a restricted region of this plane. Also, an electron's P_z and W changes little during the electron's violent gyrations in physical space. The allowed P_z-W region is bounded by an anode curve, a cathode curve, and a laminar-orbit curve (A, C, and L_s in Fig. 7). Any electron with P,W above the anode (cathode) boundary will be lost to the anode (cathode) within a single gyration. Electrons with P,W on the laminar boundary have laminar orbits at some radial distance from the cathode. This distance increases with decreasing P and W on the laminar boundary. Notice how the laminar boundary gets closer to the anode boundary with decreasing P and W. Electrons with large negative values of P and W near the laminar boundary have quasi-laminar orbits at or very near the anode radius.

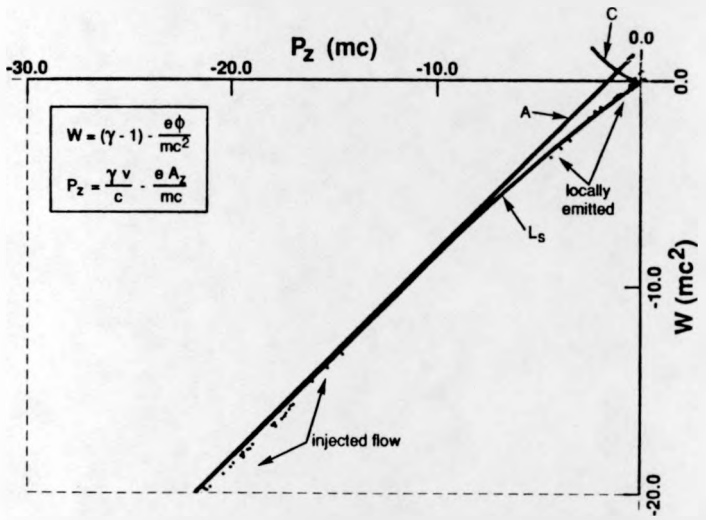

Fig. 7. Positive-polarity simulation particle plot in P_z-W plane at 22 ns. These particles occupy an axially narrow spatial bin in the final MITL.

The particle plot of Fig. 7 was computed for electrons within an axially narrow bin extending across the entire AK gap in the final MITL. Electrons that were emitted from the local cathode (LEF) are distributed near P=W=0 as in the typical single-cathode case.

Other electrons in the flow at this location were emitted from the cathodes of the adder. At the time of this plot the nearest upstream cathode is at a potential that is about 5 MV closer to the anode potential than the final MITL cathode. Because of this energy difference, these injected electrons reside farther down the laminar boundary, starting at about W = -10. As Fig. 7 shows, the injected electrons are necessarily traveling very close to the anode. The other injected electrons are correspondingly farther down the laminar boundary and are therefore injected into the flow well away from the cathode of the final MITL. Note that the injected particles shown slightly below the laminar boundary indicate the accumulated inaccuracy of the potential calculation for the laminar line plot close to the anode compared to the exact particle momentum and energy computations.

Anode and Cathode Currents

The Electron Flow Graph of Fig. 8, generated by a simulation of positive-polarity Hermes III shows, as in the negative-polarity case, that the anode current is roughly constant throughout the system; but, in going from negative to positive polarity the anode current has increased from 750 kA to 1.05 MA. Coincident with the current increase, the voltage drops to 17 MV owing to the source impedance of the disk feeds. The cathode current decreases more rapidly with the number of upstream gaps, with the corresponding electron flow (difference between anode and cathode currents) in the first sections less than in negative polarity and rapidly increasing to about double the negative-polarity value in the final MITL. Half of this electron flow is injected from the adder; the other half is the locally emitted flow which is about the same as the electron flow in the negative-polarity final MITL.

We need to learn the consequences of this additional electron flow on the operation of an ion diode. A simple theoretical model that enables us to characterize the electron flow from current measurements provides us with an important tool.

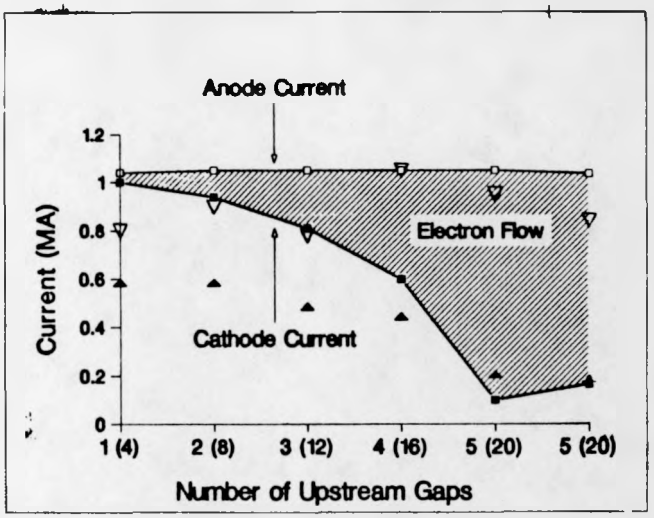

Fig. 8. Electron flow increases with number of upstream gaps in simulation of positive-polarity Hermes III. The numbers on the abscissa are spool numbers or number of upstream gaps in the simulation; the numbers in parenthases tell the corresponding number of Hermes-III gaps. The second 5(20) position is downstream of the first 5(20) position. Triangles are experimentally measured currents at peak voltage: anode (open), and cathode (solid).

Preliminary measurements on positive-polarity Hermes III[5] agree with the simulation results qualitatively; but, there are some discrepancies. As illustrated in Fig. 8, the experiment shows greater electron flow in the first sections, and the flow increases less rapidly through the adder, and then more rapidly after the final feed, reaching about 75 % of the simulation value in the final MITL. These results

need to be repeated in additional, well controlled experiments. If confirmed, it will be important to understand these discrepancies.

1-D Equilibrium MITL Theory, FGF

Knowing that the flow extends all the way to the anode in the final MITL removes one of the unknowns in the derivation of (1), thus eliminating the need for some of the assumptions. We can now return to the pressure-balance derivation[7] and derive an even simpler relationship than (1) between the anode and cathode currents and the voltage. Exploiting the knowledge that the electron flow extends across the entire gap was suggested by C. W. Mendel[15]. In planar geometry, the uniform density requires

$$\phi = \rho/\epsilon_0\, y^2/2,$$
$$\text{and, } E = \rho/\epsilon_0\, y,$$

where ϕ is the electrostatic potential, E the normal (y-component) electric field, and y is the distance across the gap from the cathode. The electron cloud that extends fully to the anode then requires that the constant charge density and MITL voltage be given by

$$\rho = \epsilon_0\, E_A/g,$$
$$\text{and, } V = \phi_A = \rho/\epsilon_0\, g^2/2,$$

where g is the AK gap of the MITL. Eliminating the electron charge density function ρ, the line voltage becomes

$$V = E_A\, g/2.$$

By pressure balance, the anode electric field is

$$E_A = c\,(B_A^2 - B_C^2)^{1/2},$$

where B_a and B_c are the anode and cathode magnetic fields. Hence, the voltage is

$$V = Z_0/2\,(I_A^2 - I_C^2)^{1/2}, \qquad (3)$$

where the planar relationships

$$B = \mu_0\, I/w, \text{ and } Z_0 = (\mu_0/\epsilon_0)^{1/2}\, g/w$$

have been used to change from geometric and field quantities to impedance and currents. Here w is the planar line width, corresponding to the circumference of a cylindrical line.

The contours computed from (3) are shown in Fig. 9 for the vacuum impedance of the final MITL of Hermes III. These equilibria predict the increased electron flow observed above 14 MV in the positive-polarity simulation. They also predict just the current increase necessary to account for the impedance decrease observed in the final MITL when the polarity is changed from negative to positive in both simulations and experiment[5,6].

The simulation tests the applicability of the FGF prescription for calculating positive-polarity MITL voltage from anode and cathode currents. The voltage is computed from (3) using the currents at the final MITL, shown in Fig. 10. The result compares favorably with the actual MITL voltage in Fig. 11. When FGF is not present, use of (3) will yield a voltage that is less than the true value.

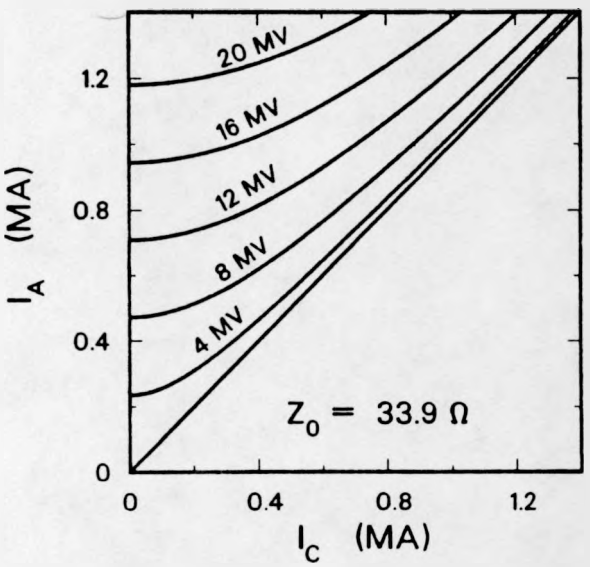

Fig. 9. Voltage contours for 1-D, planar magnetically insulated FGF equilibrium.

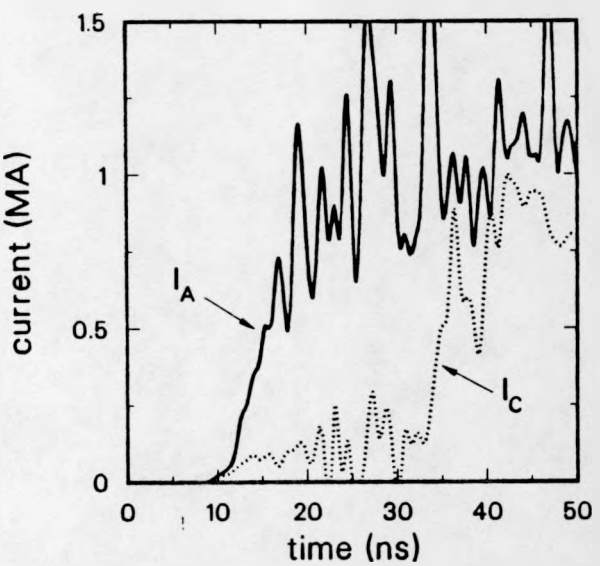

Fig. 10. Anode (solid) and cathode (dotted) current waveforms at the final MITL from positive-polarity simulation.

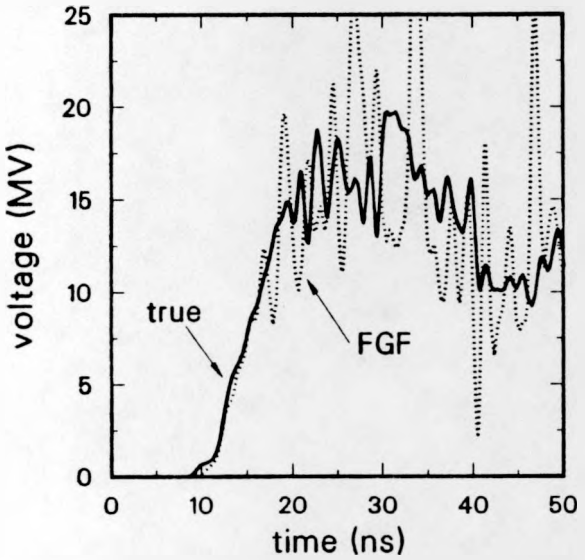

Fig. 11. Voltage (dotted) calculated from (3) using waveforms of Fig. 10 compared to true simulation voltage (solid) at final MITL.

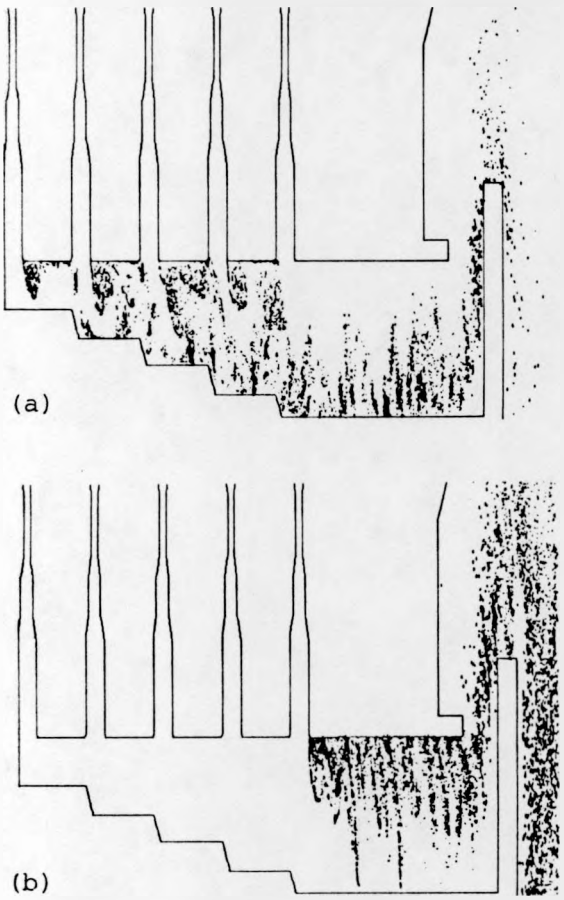

Fig. 12. Positive-polarity simulation z-r particle plots showing (a) the injected flow from the adder cathodes, and (b) the locally emitted flow of the final MITL.

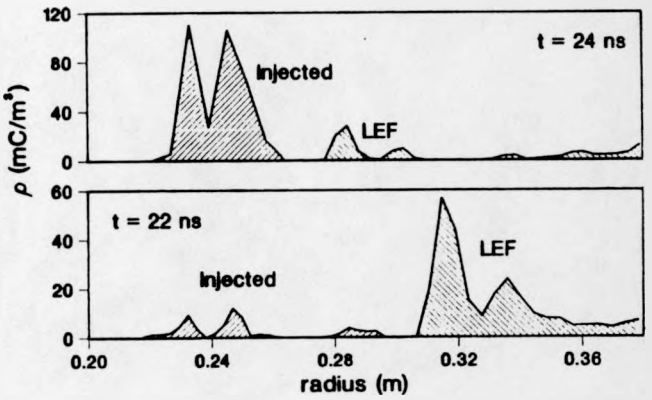

Fig. 13. In the final MITL the locally emitted flow (LEF) remains radially distinct from the injected flow. The radial profile, distinguishing both flow components, is plotted at 22 and 24 ns.

1-D Equilibrium MITL Theory, LEF

In the simulation we have labeled the electrons according to their cathode of origin. Returning to the simulation particle plot, we can separate out the injected flow to see its spatial relationship to the locally emitted flow in Figs. 12a and b. All particles are present in each plot; but, only the particles emitted from the adder cathodes are visible in Fig. 12a, and only those emitted from the final MITL cathode are visible in Fig. 12b. As suggested by the vacuum equipotentials, the injected flow does indeed remain radially separate from the locally emitted flow. There are only occasional departures from this stratified equilibrium as indicated by the two spikes in the locally emitted flow shown at this time.

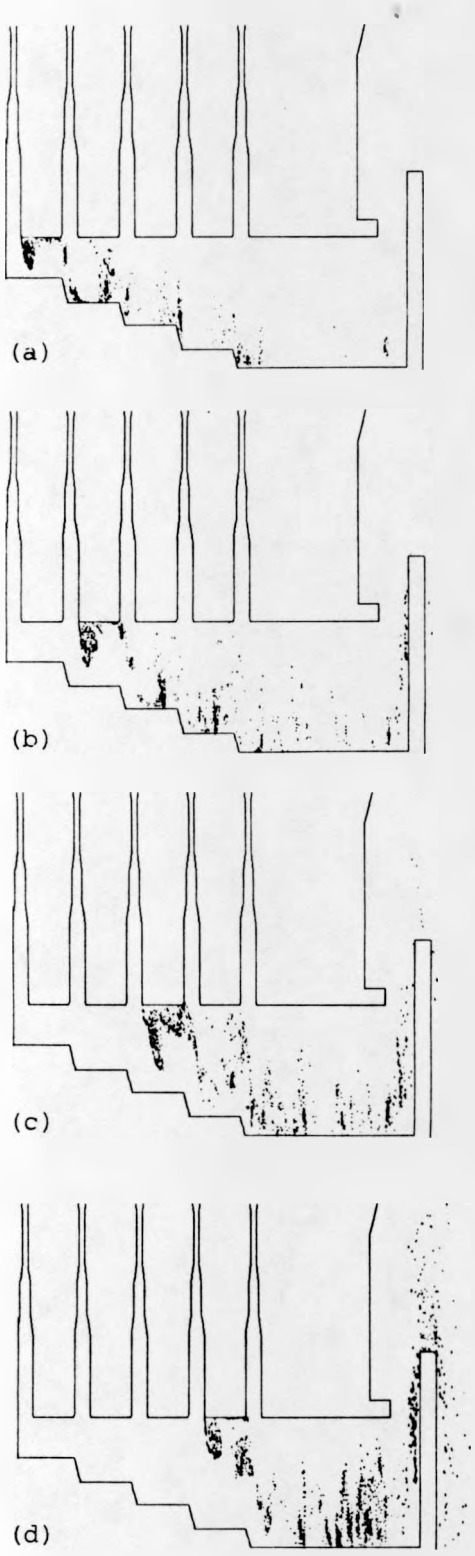

Fig. 14. Positive-polarity simulation z-r particle plots at 22 ns showing each component constituting the injected flow: electrons from the cathode just following (a) the 1st disk feed, (b) the 2nd, (c) the 3rd, and (d) the 4th disk feed.

The contributions of both injected and locally emitted electrons to the radial charge density profile in the final MITL illustrate in Fig. 13 how drastically the injected component can change during several ns, although it remains separate from the locally emitted component. The radial profile of the injected component is known to be unstable[16], and this feature will be investigated in future work. Separately viewing each component of the injected flow of Fig. 12a shows in Figs. 14a through d that these components are not themselves radially layered, owing to the turbulence in the adder MITL.

Since there is essentially no mixing of the locally emitted and injected flows in the final MITL, we could also use the single-cathode 1-D theory that was successful in negative polarity. In this case, rather than using the final-MITL anode and cathode currents whose difference is the total flow, we use two cathode currents (e.g., at the final MITL and just downstream of the 4th radial feed of Fig. 2) whose difference is just the locally emitted flow.

Comparing the magnitude of the mean locally emitted electron density profile indicated by Fig. 13 with the value from (2) (using the cathode current of Fig. 10 at 22 and 24 ns), suggests that the second term of (1) will sometimes be too large, giving momentary deficiencies in the voltage calculated by (1). Such deficiencies occur in the LEF calculated voltage at times when radial charge spikes such as indicated in Fig. 12 go by the current diagnostic position. The charge spikes give nonequilibrium jumps in the locally emitted flow current. Momentary dropouts in the LEF calculated voltage do indeed occur in the simulation; however, the envelope of the LEF voltage matches the true simulation voltage well. Note that when FGF exists, the FGF calculation should not be sensitive to spikes in the locally emitted flow.

Voltage Calculated from Hermes-III Data

The simulations have suggested that we can use simple 1-D theory in two different ways to calculate voltage from the currents, and the two approaches should agree to the extent that (1) there is full-gap flow, and (2) the injected flow and locally emitted flow do not radially mix.

Both techniques applied to positive-polarity Hermes-III data give voltage waveforms that agree closely. Figure 15 shows two examples of voltage vs. time plots computed from current measurements on positive-polarity Hermes III. The agreement between the two methods shown in each example indicates that full-gap flow and radial separateness between the injected and locally emitted flows occured in the actual experiment.

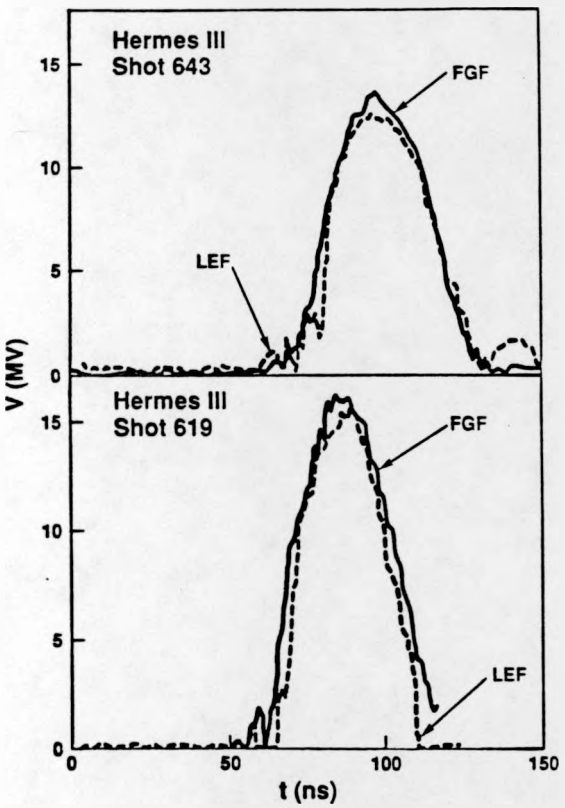

Fig. 15. Comparison of FGF and LEF voltages calculated from current waveforms measured on two different Hermes-III shots.

Summary

The simulations have established that calibrated current measurements on positive-polarity Hemes III can be used to diagnose two important features of the electron flow. They indicate whether the flow extends over the entire gap of the transmission line at the high-voltage end of the accelerator, and whether the electrons injected into this flow from lower-voltage cathodes mix with the electrons emitted from the cathode of the final transmission line.

Typically the injected electrons comprise about half the electron flow current in the final transmission line; and, although their flow is turbulent, they travel primarily near the anode, separate on average from the electrons emitted by the final cathode. Learning the consequences of this large and turbulent injected electron flow on the operation of an applied-B extraction ion diode is an important issue of light ion inertial confinement fusion research.

Acknowledgements

I would like to thank C. W. Mendel, Jr. for useful discussions, J. P. Corley and D. L. Johnson for their Hermes-III and HELIA data, and J. J. Ramirez for his interest in this effort.

This work was supported by the U.S. Department of Energy under contract DE-AC04-76DP00789.

References

[1] J.J. Ramirez, et. al., "The Four Stage HELIA Experiment", Proc. of the 5th IEEE Pulsed Power Conf., Arlington, VA, June 10-12, 1985, p. 143.

[2] J.J. Ramirez, et. al., "The Hermes III Program", Proc. of the 6th IEEE Pulsed Power Conf., Arlington, VA, June 29-July 1, 1987, p. 294.

[3] J.J. Ramirez, et. al, "Performance of the Hermes-III Gamma Ray Simulator", Proc. of the 7th IEEE Pulsed Power Conf., Monterey, CA, June 11-14, 1989, p. 26.

[4] I. Smith, et. al., "Design of a Repetitive +30 MV, 4 MJ, 9 ns ICF Reactor Driver", Proc. of the 7th IEEE Pulsed Power Conf., Monterey, CA, June 11-14, 1989, p. 36.

[5] D.L. Johnson, et. al., "Hermes-III Positive Polarity Experiment", Proc. of the 7th IEEE Pulsed Power Conf., Monterey, CA, June 11-14, 1989, p. 32.

[6] J.P. Corley, et. al., "Positive Polarity Voltage Adder MITL Experiments on HELIA", Proc. of the 7th IEEE Pulsed Power Conf., Monterey, CA, June 11-14, 1989, p. 571.

[7] C.W. Mendel, Jr., D.B. Seidel, and S.E. Rosenthal, "A Simple Theory of Magnetic Insulation from Basic Physical Considerations", Laser and Particle Beams, vol. 1(3), p. 311, 1983.

[8] P.A. Miller and C.W. Mendel, Jr., "Analytic Model of Applied-B Ion Diode Impedance Behavior", J. Appl. Phys., vol. 61(2), p. 529, January, 1987.

[9] S.E. Rosenthal and C.W. Mendel, "Simple Equilibrium Theory for Coaxial Magnetically Self-Insulated Flow", Bull. Am. Phys. Soc., vol. 30, p. 1534, October, 1985; S.E. Rosenthal and C.W. Mendel, Jr., "Coaxial MITL Theory", Particle Beam Fusion Progress Report July through December 1985, Sandia National Laboratories, Albuquerque, NM, SAND86-0016, p. 59, December, 1987.

[10] R.I. Lawconnell and J. Neri,"Theory of Magnetically Insulated Electron Flows in Coaxial Pulsed Power Transmission Lines", Phys. Fluids B, vol. 2(3), p. 629, March 1990.

[11] B. Goplen, et. al., "User's Manual for MAGIC / Version - September 1983", Mission Research Corporation Report No. MRC/WDC-R-068, Alexandria, VA, September, 1983; T.D. Pointon, "A Method for Handling Slanted Conducting Surfaces in EM PIC Codes", SAND88-0982 UC-28, Sandia National Laboratories, Albuquerque, NM, June, 1988.

[12] J.M. Creedon, "Magnetic Cutoff in High-Current Diodes", J. Appl. Phys., vol. 48, p. 1070, March, 1977.

[13] D.E. Hasti, et. al., "HELIA--High Energy Linear Induction Accelerators", IEEE Power Modulator Symposium, June 18-20, 1984, p. 299; J.W. Poukey, "Hermes and HELIA

Simulations, 1988", SAND88-3138 UC-28, Sandia National Laboratories, Albuquerque, NM, February, 1989.

[14] C.W. Mendel, Jr., D.B. Seidel, and S.A.Slutz, "A General Theory of Magnetically Insulated Electron Flow", Phys. Fluids, vol. 26(12), p. 3628, December, 1983.

[15] C.W. Mendel, Jr., private communication.

[16] R.C. Davidson, "Quasilinear Theory of the Diocotron Instability for Nonrelativistic Non-neutral Electron Flow in Planar Geometry", Phys. Fluids, vol. 28(6), p. 1937, June, 1985.